Clim Dyn
DOI 10.1007/s00382-017-3720-z

Predictability and prediction of the total number of winter extremely cold days over China

Xiao Luo[1] · **Bin Wang**[1,2]

Received: 28 October 2016 / Accepted: 2 May 2017

Abstract The current dynamical climate models have limited skills in predicting winter temperature in China. The present study uses physics-based empirical models (PEMs) to explore the sources and limits of the seasonal predictability in the total number of extremely cold days (NECD) over China. A combined cluster-rotated EOF analysis reveals two sub-regions of homogeneous variability among hundreds of stations, namely the Northeast China (NE) and Main China (MC). This reduces the large-number of predictands to only two indices, the NCED-NE and NCED-MC, which facilitates detection of the common sources of predictability for all stations. The circulation anomalies associated with the NECD-NE exhibit a zonally symmetric Arctic Oscillation-like pattern, whereas those associated with the NECD-MC feature a North–South dipolar pattern over Asia. The predictability of the NECD originates from SST and snow cover anomalies in the preceding September and October. However, the two regions have different SST predictors: The NE predictor is in the western Eurasian Arctic while the MC predictor is over the tropical-North Pacific. The October snow cover predictors also differ: The NE predictor primarily resides in the central Eurasia while the MC predictor is over the western and eastern Eurasia. The PEM prediction results suggest that about 60% (55%) of the total variance of winter NECD over the NE (Main) China are likely predictable 1 month in advance. The NECD at each station can also be predicted by using the four predictors that were detected for the two indices. The cross-validated temporal correlation skills exceed 0.70 at most stations. The physical mechanisms by which the autumn Arctic sea ice, snow cover, and tropical-North Pacific SST anomalies affect winter NECD over the NE and Main China are discussed.

Keywords East Asian winter monsoon · Extreme weather events · Extremely cold days · Seasonal predictability · Physical-empirical model (PEM)

1 Introduction

During the winters of 2007/2008 and 2009/2010, China had experienced extremely cold weather (Wen et al. 2009; Zhou et al. 2009; Wang and Chen 2010). Cold surges and blizzard freezing rain resulted in heavy economic losses. In other occasions, however, a cold air outbreak can alleviate hazes in heavily polluted industrial cities. Forecasting extremely cold weather is thus of paramount importance for China where the world strongest East Asian winter monsoon (EAWM) prevails.

Dynamical seasonal prediction of winter mean temperature remains a great challenge regardless of prominent progresses that have been made in understanding the interannual variability and prediction of the EAWM (Wang et al. 2010; Wang and Lu 2016). By analyzing the 22-year multi-model hindcast datasets from the CliPAS and DEMETER projects, Lee et al. (2013) found that dynamical prediction of seasonal mean temperature anomaly over the continental Asian monsoon region has poor skills.

To further assess the dynamical models' prediction skills over Asia, we have examined a 46-year (1960–2005)

✉ Bin Wang
Wangbin@hawaii.edu

[1] Department of Atmospheric Sciences and Atmosphere-Ocean Research Center, University of Hawaii at Manoa, Honolulu, HI 96822, USA

[2] Earth System Modeling Center, Nanjing University of Information Science and Technology, Nanjing 210044, China

Published online: 09 May 2017

retrospective forecast results made by five models from the ENSEMBLE project (details are introduced in Sect. 2.1). We find that the multi-model ensemble (MME) prediction has notoriously low skills over China where the domain-averaged and latitude-weighted temporal correlation skill for the 46-year period is only 0.23 (Fig. 1). This confirms that China is a region of great challenge for winter temperature prediction. Therefore, it is difficult to use the current dynamical models to estimate the potential predictability for winter mean temperature.

Apart from the winter mean temperature, prediction of extremely cold events has attracted increasing attention. Similar to the seasonal mean prediction, dynamical models also lack skills in prediction of winter extremes. Pepler et al. (2015) have shown that the skill of a multi-model ensemble forecast of 10th percentile of daily minimum temperature is statistically insignificant over the mid- and low- latitude East Asia. Previous studies have suggested a high correlation between the seasonal mean temperature and the number of extremely cold day (ECD) (Collins et al. 2000). This relationship was found to be valid in the recent effort in prediction of ECD numbers over the temperate East Asia (Luo and Wang 2016). Whether this relationship can apply to the entire China and to what extent the ECD in China are predictable remain unclear.

Based on the EAWM indices that represent the winter temperature anomalies over China, some studies have found that the winter monsoon could be predicted to some extent by using statistical prediction methods (Liu et al. 2012; Sun et al. 2014; Wang and Chen 2014; Yang and Lu 2014). Among these studies, the sea surface temperature anomalies over the Pacific region, Arctic sea ice concentration anomalies, and snow cover anomalies are found to be useful precursors. However, the predictability of winter temperature and the total number of winter extremely cold days (NECD), as well as their potential regional differences over China have not been addressed.

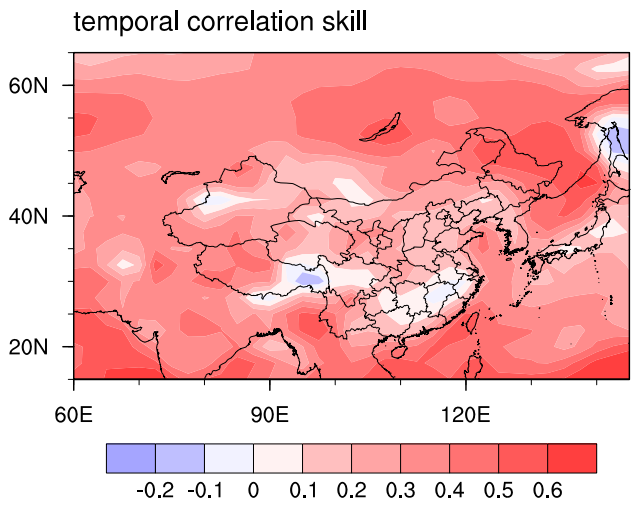

Fig. 1 Temporal correlation coefficient skill for a 1-month lead prediction of the winter 2 m air temperature obtained from the ENSEMBLE multi-model ensemble (MME) hindcast for the of 1960–2005. The TCC skill averaged over the entire China is 0.23

To what extent can we predict the winter NECD before the beginning of a winter season? In this study, we focus on understanding the physical processes that govern the lead-lag correlation between the precursors and the frequency of winter extremely events for seasonal forecast. We will use a physics-based empirical model (PEM) approach to estimate the predictability of the NECD because the dynamical models have inadequate hindcast skills. The PEM approach has been successfully applied to the estimations of seasonal predictability of summer rainfall anomalies over India (Wang et al. 2015; Li and Wang 2015) and East Asia (Yim et al. 2014; Xing et al. 2014, 2017), as well as the annual minimum Arctic sea ice extent anomalies (Grunseich and Wang 2016). Section 2 describes the datasets used and methodology. Section 3 introduces division of the sub-regions with homogeneous NECD variability in China. Section 4 presents characteristics of NECD-related simultaneous winter circulation anomalies. In Sect. 5, we search for physically consequential predictors and followed by discussing the mechanisms by which the selected predictors affect NECD in the corresponding regions. Section 6 establishes the PEMs for the NE and MC to estimate the predictability of NECD for each derived region. The last section summarizes major results and discusses related issues.

2 Data and methodology

2.1 Datasets

This study uses daily mean temperature data from 503 Chinese weather stations that have no missing data during winter. The analysis period is 41 winters from 1973/1974 to 2013/2014 during which snow cover data are available. For simplicity, the winter of 1973 refers to the December 1973 to February 1974. Daily and monthly circulation data are from the National Centers for the Atmospheric Research (NCEP-NCAR) reanalysis (Kalnay et al. 1996). The SST data gridded at 2° × 2° resolution are derived from the National Oceanic and Atmospheric Administration (NOAA) extended reconstructed SST (ERSST version 3b) (Smith et al. 2008). The weekly snow cover extent data are obtained from the Global Snow Laboratory (Rutgers University). In addition, monthly mean precipitation data are adopted from Global Precipitation Climatology Project (GPCP) version 2.2 dataset for the period of 1979–2013 (Huffman and Bolvin 2013). Since trends caused by external forcing or governed by different mechanisms can be

found in both predictors and predictands, for consistency, in this study we removed the linear trends from all seasonal and monthly mean fields when identifying precursors and establishing PEMs.

The hindcasts made by the ENSEMBLES project for the period of 1960–2005 (Weisheimer et al. 2009) were used to assess the performance of the dynamical models. This data set consists of five state-of-the-art coupled atmosphere ocean circulation models, i.e., the Euro-Mediterranean Center for Climate Change (CMCC-INGV) in Bologna, European Centre for Medium-Range Weather Forecasts (ECMWF), the Leibniz Institute of Marine Sciences at Kiel University (IFM-GEOMAR), Météo France (MF), and UK Met Office (UKMO). The hindcasts were initiated form Nov. 1st that yielded an 1-month-lead winter season (December to February, or DJF) forecast. The multi-model ensemble (MME) prediction was made by simply averaging the above five models' hindcasts.

2.2 Cluster analysis and Rotated EOF analysis

To determine regions with relatively homogeneous variations, we used a combined k-means cluster analysis (Wilks 2011) and rotated EOF (REOF) analysis (Richman 1986) algorithm. The Euclidean distance used in the k-means cluster analysis helps to find an optimal partition of the whole data into k clusters. The members within each cluster have similar variations, but the members among different clusters have as much different variations as possible. For the k-means method, the clustering result is subject to the initial grouping, and the final partition can be sensitive to such an initial grouping. Therefore, the algorithm is repeated 200 times, each time with different initial centroids, in order to find the most appropriate result that minimizes the sum of the squared distances between the cluster members and their respective cluster centroids (Philipp et al. 2007).

"Rotation" transforms the Empirical Orthogonal Function into a non-orthogonal linear basis, and results in "Rotated EOFs" that can be more easily interpreted than conventional EOFs (Storch and Zwiers 2001). Based on the results of Cluster and REOF analyses, we will be able to determine the regional modes and the corresponding indices that are defined as distinguished predictands.

2.3 Numerical model and experimental design

Numerical experiments are conducted to understand the possible physical processes linking the autumn tropical-North Pacific SST anomaly and the ensuing winter NECD in China. The coupled model used is the Nanjing University of Information Science and Technology coupled Earth System Model (NUIST-ESM) v1a (Cao et al. 2015). This NUIST-ESM consists of an atmospheric component using version 5.3 of the European Centre Hamburg Model (ECHAM), an oceanic component using version 3.4 of the Nucleus for European Modeling of the Ocean (NEMO), and a sea ice component using version 4.1 of the Los Alamos sea ice model (CICE). The NUIST-ESM has been used to study the dynamical processes that impact the Indian summer monsoon rainfall (Li et al. 2016).

Two sets of paired experiments are performed to evaluate the impact of the autumn Pacific SST anomaly on the ensuing winter circulation. In the first set of experiments, the model SST anomaly field is nudged toward the prescribed SST anomaly associated with the SST precursor. The nudging starts from September 1st, and ends on October 31st. The nudged SST anomalies with opposite polarities are used in the second set of experiments. The two sets of experiments with SST nudging are denoted as (+) SST and (−) SST run, respectively. Each set of experiments consists of 30 ensemble members, and the differences between the (+) SST and (−) SST experiments' ensemble means are used to analyze the wintertime circulation anomalies induced by the SST precursors.

3 Leading regional modes of NECD in China

The NECD is defined for each station, which is the accumulative number of the ECDs (NECD) during winter. The ECD is defined as the lower 10th percentile of the daily mean temperature at each station [refer to Luo and Wang (2016)].

Predicting climate extremes in a large domain such as China involves hundreds of stations (or grids). In the present study, we first apply the combined cluster-rotated EOF analysis to identify regions in which NECD variations are relatively homogeneous, thus a single, area-mean NECD can be defined as a predictand for this "regional mode". Mathematically, the complex problem of prediction of the NECDs at individual stations (high-dimensional predictand) is reduced to a simple problem of prediction of a few regional indices (low-dimensional predictand) that quantify the variabilities of each regional mode. Physically, this approach will greatly facilitate understanding the sources of predictability and detecting large-scale predictors. Practically, as will be demonstrated in Sect. 6, the NECD at each station can be conveniently predicted by using only a few large-scale predictors that were identified for the regional modes.

Cluster analysis is used to identify sub-regions of the relatively homogeneous variations in NECDs. A critical question in cluster analysis is how many clusters should be chosen. Statistically, one can use the squared distance as a criterion. The square distance deceases when the number

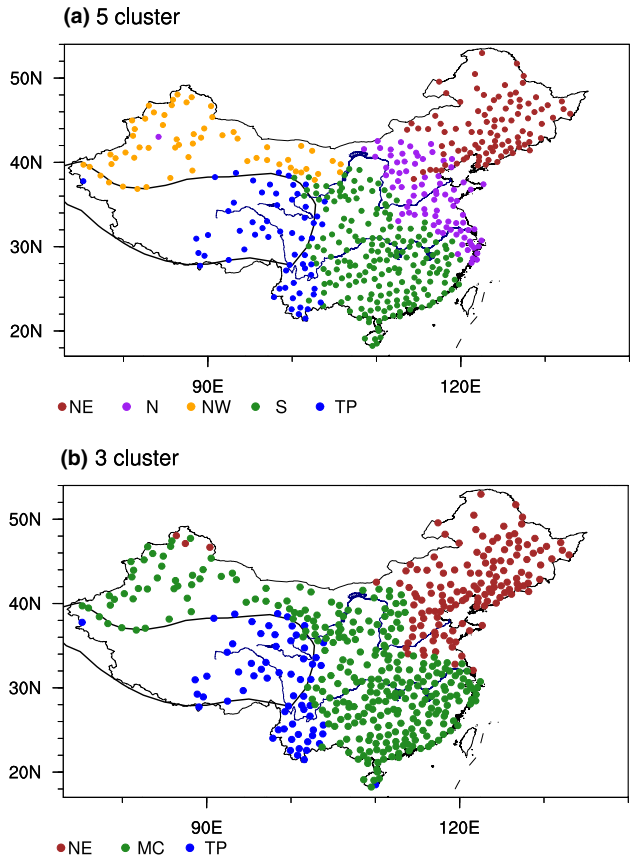

Fig. 2 Distribution of the winter climate zones in China as detected by a cluster analysis of the extremely cold days (ECDs) observed over 503 weather stations. Results are shown for an optimum **a** five-cluster and **b** three-cluster analysis. *Dots* represent locations of the stations. The *black line* is the 3000 m height contour, indicating the location of the Tibetan Plateau. The symbols NE, N, NW, S, MC and TP represent the Northeast China, North China, Northwest China, Central-South China, Main China, and Tibetan Plateau area, respectively

of cluster increases. Thus, when a marked drop occurs between the two adjacent cluster numbers (for instance, n and n + 1), one may choose n + 1 as an appropriate cluster number. Unfortunately, in our case, no notable drop was found from cluster 1 to cluster 10. However, the cluster 3 and cluster 5 exhibit relatively large drops (figure not shown). For this reason, we compared these two choices. The geographical maps of sub-region distribution that resulted from the 5- and 3- cluster analysis are shown in Fig. 2. To find out which classification of the above two is more adequate for representing distinguished regional modes, we first define the mean NECD averaged over all stations (cluster members) in a sub-region (cluster) as a regional index, and then make a correlation analysis of the regional indices. The results of the 5-cluster analysis show that the NECDs in the Central-South China and Northwest China, and the NECDs in the North China and Northeast China are both significantly correlated with each other (Table 1a). In addition, both the NECD in the Central-South China and North China are highly correlated with that in the Northwest China. Obviously, the five regional modes are not sufficiently independent predictands. In sharp contrast, the regional indices derived from the 3-cluster analysis are more mutually independent (Table 1b). For the purpose of forecasting, the division of three sub-regions is found to be optimal.

The cluster analysis results are further compared with the results of REOF analysis. The first three EOFs are retained and subjected to the varimax rotation. As shown in Fig. 3, the first two spatial patterns of the REOFs reflect the same regional distribution as Main China and Northeast China detected by the 3-cluster analysis, confirming the robustness of categorization of the NE and MC. However, the third REOF shows a large loading over the south and southwestern China, which is inconsistent with the domain of TP region described by the 3-cluster analysis. Considering the high topography over the plateau region, as well as

Table 1 The correlation coefficients between any two of the NECD indices within the different cluster groups during 1973–2013

(a)	NECD-TP(5)	NECD-NE(5)	NECD-S(5)	NECD-NW(5)	NECD-N(5)	NECD-MC(3)
NECD-TP(5)	1	−0.04	0.39	0.09	0.15	0.33
NECD-NE(5)		1	0.32	0.34	**0.70**	0.38
NECD-S(5)			1	**0.64**	**0.73**	**0.98**
NECD-NW(5)				1	**0.57**	**0.78**
NECD-N(5)					1	**0.79**
(b)		NECD-TP(3)		NECD-NE(3)		NECD-MC(3)
NECD-TP(3)				−0.01		0.37
NECD-NE(3)						**0.48**
NECD-MC(3)						

The bold numbers are statistically significant at 99% confidence level. The number in the bracket denotes the index belongs to 5-cluster zones or 3-cluster zones. (a) Correlations between NECD indices from 5-cluster (b) Correlations between NECD indices from 3-cluster

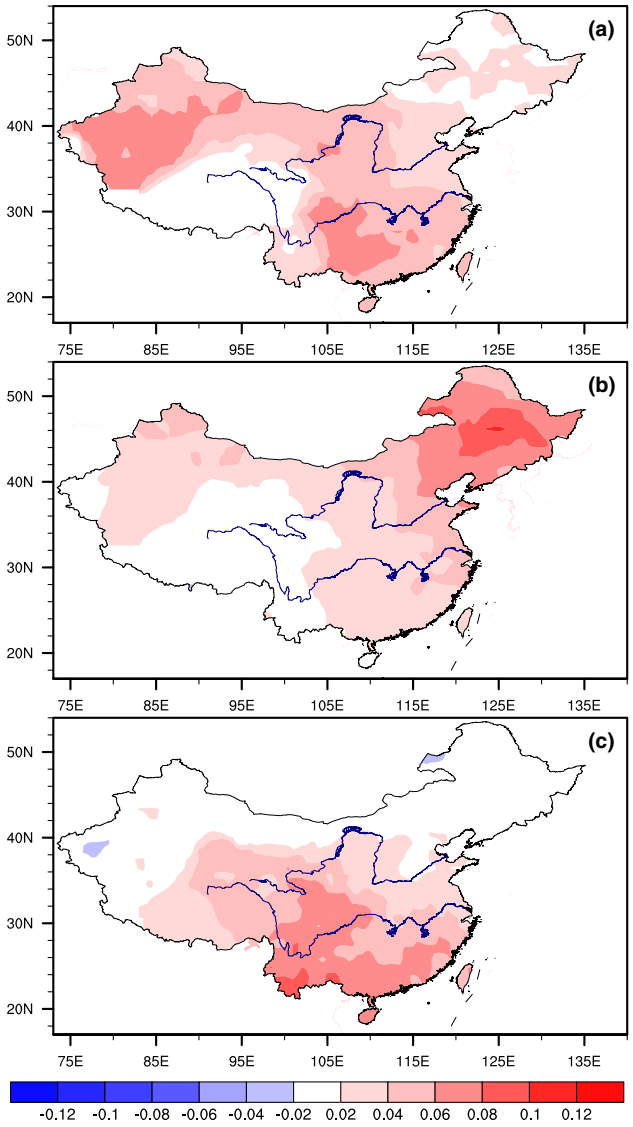

Fig. 3 Spatial patterns of the first three modes of the NECD over 503 Chinese weather stations derived by REOF analysis

the difference between REOF and cluster analyses, we only focus on the ECDs occur in the NE and MC regions. The ECDs in the TP region will be discussed separately elsewhere. In this study, the predictands are defined as area-averaged NECD for the NE and MC regions (Indices), i.e., NCED-NE and NCED-MC, respectively.

Figure 4 shows the time series of the non-detrended NECD-NE and NECD-MC. Over the past 41 years, the linear trend of the NECD-NE is −0.91 day per decade, and this trend is significant at the 89% confidence level ($p=0.89$). Similarly, the NECD-MC has a trend of −0.93 day per decade for ($p=0.87$). Although the significance level is lower than 90%, there is a moderate trend in both the NECD-MC and NECD-NE. Both indices display a multi-decadal variation with a low-NECD (or warm winter) period from 1986 to 2006 and followed by a rebound since the early 2000s, corresponding to the decadal variations of the EAWM (Wang and Chen 2013). The indices for the two climate zones display similar spectral peaks at 3 and 2.5 years, respectively, which are marginally significant at the 95% confidence level. The two detrended NECD-NE and NECD-MC indices will be our target predictands.

4 Characteristic circulation anomalies associated with the NECD in NE and main China

It is a natural starting point to find out what the major anomalous circulation systems are when more ECDs occur in the NE and MC regions. Figure 5a shows that more frequent occurrence of ECD in the NE China region implies a continental scale cold winter covering the high-latitude (western and central Siberia) and the far East Asia (Fig. 5a). For the MC region, more ECD are associated with a large scale of coldness over the mid-latitude and subtropical Asia except the TP (Fig. 5d). Due to the specific latitudinal location of the NE China, the circulation anomalies in winter with more ECDs are closely associated with the so-called "northern mode" of a cold East Asian winter monsoon (Wang et al. 2010; Luo and Zhang 2015), meanwhile for the MC, the higher NECD-MC related circulation anomalies are more closely associated with the EAWM "southern mode".

Generally, the winter circulation anomalies associated with higher NECD-NE are characterized by (a) a northwestward shift of the Mongolian-Siberian High and an enhanced Aleutian Low at sea level pressure field (SLP) (Fig. 5b); (b) an enhancement and the southwestward displacement of the mid-tropospheric East Asian trough that normally extends from Okhotsk Sea to Yangtze River delta and an enhancement of the Ural Mountain ridge on the 500 hPa level (Fig. 5c). The circulation anomalies of an increased NECD-NE resemble a negative phase of the Arctic Oscillation (AO). In fact, the correlation coefficient between AO index (Thompson and Wallace 1998) and the NECD-NE is −0.62, significant at the 99% confidence level.

In contrast, the circulation anomalies associated with a high NCED-MC is characterized by a meridional dipole pattern over the Eurasian continent. The negative SLP anomalies over South Asia and Indian Ocean and positive SLP anomalies over the central Eurasian continent form a "North-high and South-low" pattern which facilitates the cold air intrusion into the South China (Fig. 5e). On the 500 hPa level, the dipole anomalies also feature high anomalies over Ural regions and zonally elongated low anomalies over the subtropical regions (Fig. 5f). Different from the circulation anomalies associated with the NECD-NE,

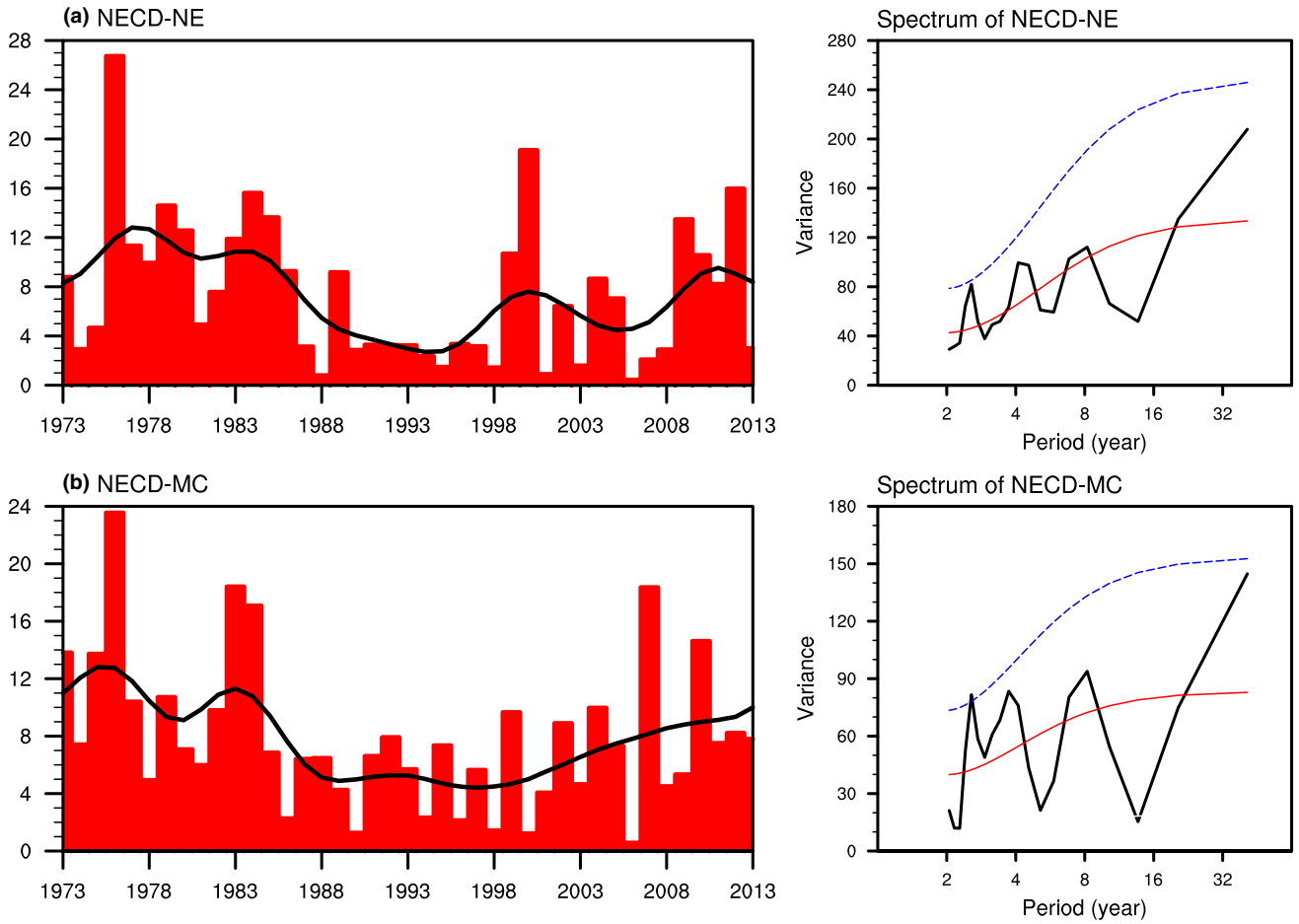

Fig. 4 Time series of the **a** NECD-NE and **b** NECD-MC indices and their corresponding power spectra. The *black lines* in the *left panels* represent their decadal components obtained by applying a 10-year low-pass filter on the time series. The *red lines* in the *right panels* indicate "*red noise*" spectra and the *blue dashed lines* indicate the 90% confidence bounds

anomalous cooling can be found over the tropical Pacific associated with more NECD-MC (Fig. 5a, d).

5 Sources of the predictability for the number of extremely cold days in China

For the PEM prediction, it is essential to understand the sources of predictability, i.e., the physical processes and mechanisms linking the predictors and predictand (Wang et al. 2015). In this section, we first describe how we find the predictors and followed by a discussion of their physical linkage to the predictands.

5.1 Different predictors for the northeast and Main China regions

Rather than fishing statistical predictors in a variety of oceanic and atmospheric fields, we examine only SST and snow cover anomalies since these variables represent lower boundary forcing conditions(Wang et al. 2015). In addition, we focus on only two types of precursors, i.e., the persistent signals in autumn represented by the seasonal or bimonthly means and tendency signal across autumn from September to November (November minus September). To determine the most meaningful predictors for each NECD regional mode, we used lead correlation coefficient (LCC) maps of the persistent and tendency fields of the SST and snow cover extensions with reference to the winter NECD indices. Particular attention is paid to the identification of the large-scale coherent LCC regions where the correlations are largely significant at the 95% confidence level.

5.1.1 SST predictors

We found that the NECD-NE and NECD-MC have different SST predictors. For the NECD-NE, the most significant precursory SST signal is the September–October (SO) mean SST anomalies in the western Eurasian Arctic Ocean (75°N–85°N, 30°E–90°E), i.e., north of the

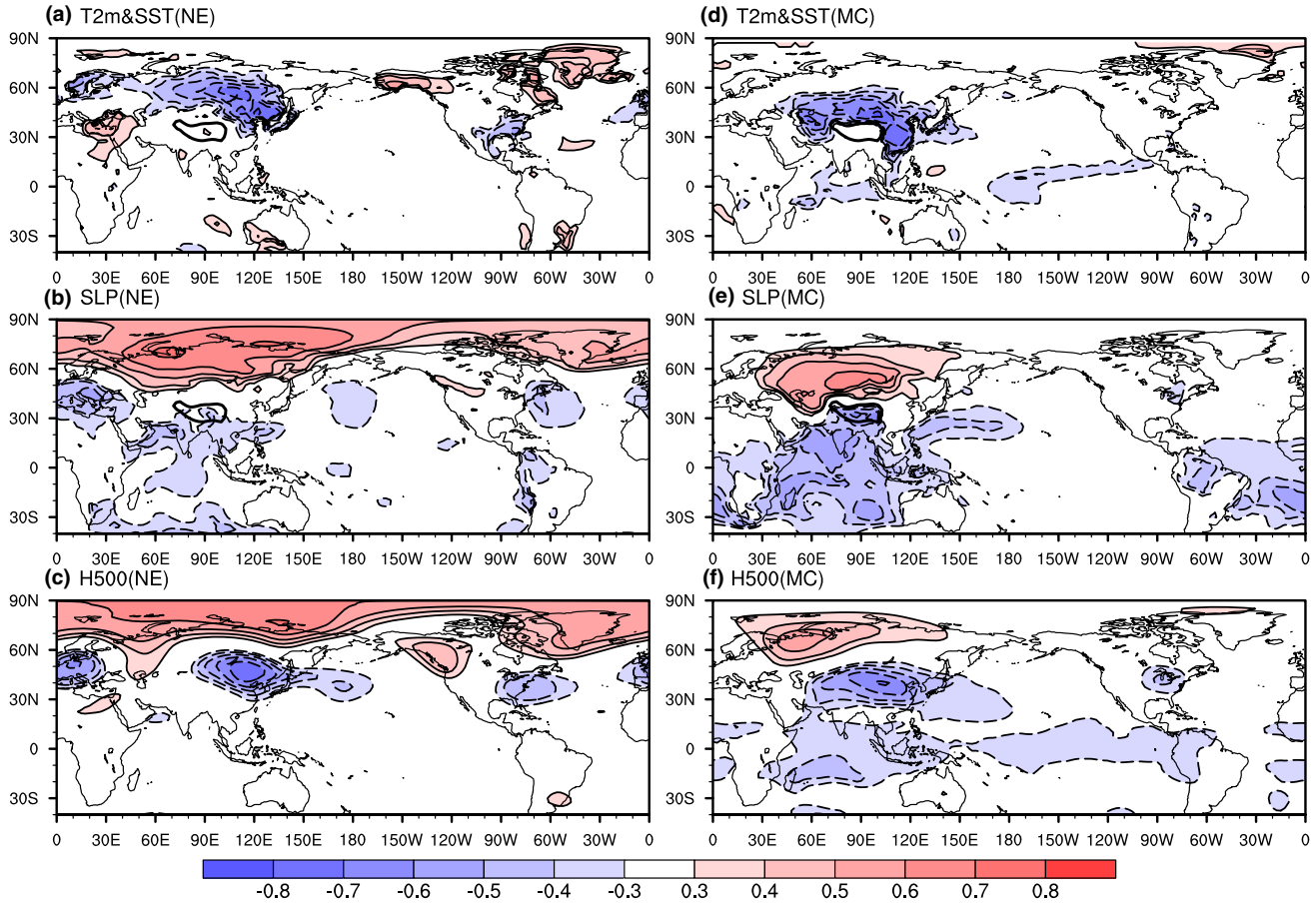

Fig. 5 Winter circulation anomalies associated with the NECD over the NE (*left panels*) and MC (*right panels*). Shown are the concurrent correlation maps between the NECD indices and the corresponding **a, d** 2 m air temperature (T2m) over land and SST over oceans, **b, e** SLP, and **c, f** 500 hPa geopotential height (H500). *Shadings* indicate the regions with correlations significant at the 95% confidence level

Barents and Kara sea regions, named as ARCT-NE for short (Fig. 6a; Table 2). This Arctic precursor is further confirmed by LCC map associated with the sea ice concentration, as significant reduced sea ice anomalies can be found over the same Arctic region (Fig. 6b). In contrast to the NE, the most significant precursory SST signal for the NECD-MC is the SO mean SST anomalies in the tropical and North Pacific (10°S–50°N, 150°E–130°W), named as TNPSST-MC (Fig. 6c; Table 2).

Following the method used by Lee et al. (2013), the SST predictor values are calculated based on the weighted averaged SST anomalies over all statistically significant grid points [coefficient coefficients reaching over (below) 0.3(−0.3) in our cases] within the selected predictor domain. The grid-point weights are provided by the correlation coefficients on LCC map. For instance, the Arctic SST predictor is calculated based on the weighted average of SO SST anomalies within the outlined box in Fig. 6a. ARCT-NE is then defined as the weighted average of SO SST anomaly divided by its standard deviation. The definition of TNPSST-MC is the same as ARCT-NE except using the weighted SST within the outlined box in Fig. 6c.

5.1.2 *Snow cover predictors*

We also found that both the winter NECD at the NE and MC are strongly foreshadowed by Eurasian snow cover anomalies in the preceding October. However, the domains of significant correlations have important differences (Fig. 6d, e). For the NECD-NE the snow cover precursory region is region A + B + C (40°N–65°N, 40°E–140°E) whereas for the NECD-MC the precursory region only covers region A + C (Fig. 6d, e). Similar to the SST predictors, the snow cover predictor for the NECD-NE (NECD-MC) is defined as weighted snow cover extension anomalies within the outlined regions A + B + C (A + C) in Fig. 6d, e. The two identified snow cover predictors are named as SNOW-NE and SNOW-MC for short (Table 2). The winter NECDs are most significantly correlated with snow cover extension anomalies in October comparing with those in September

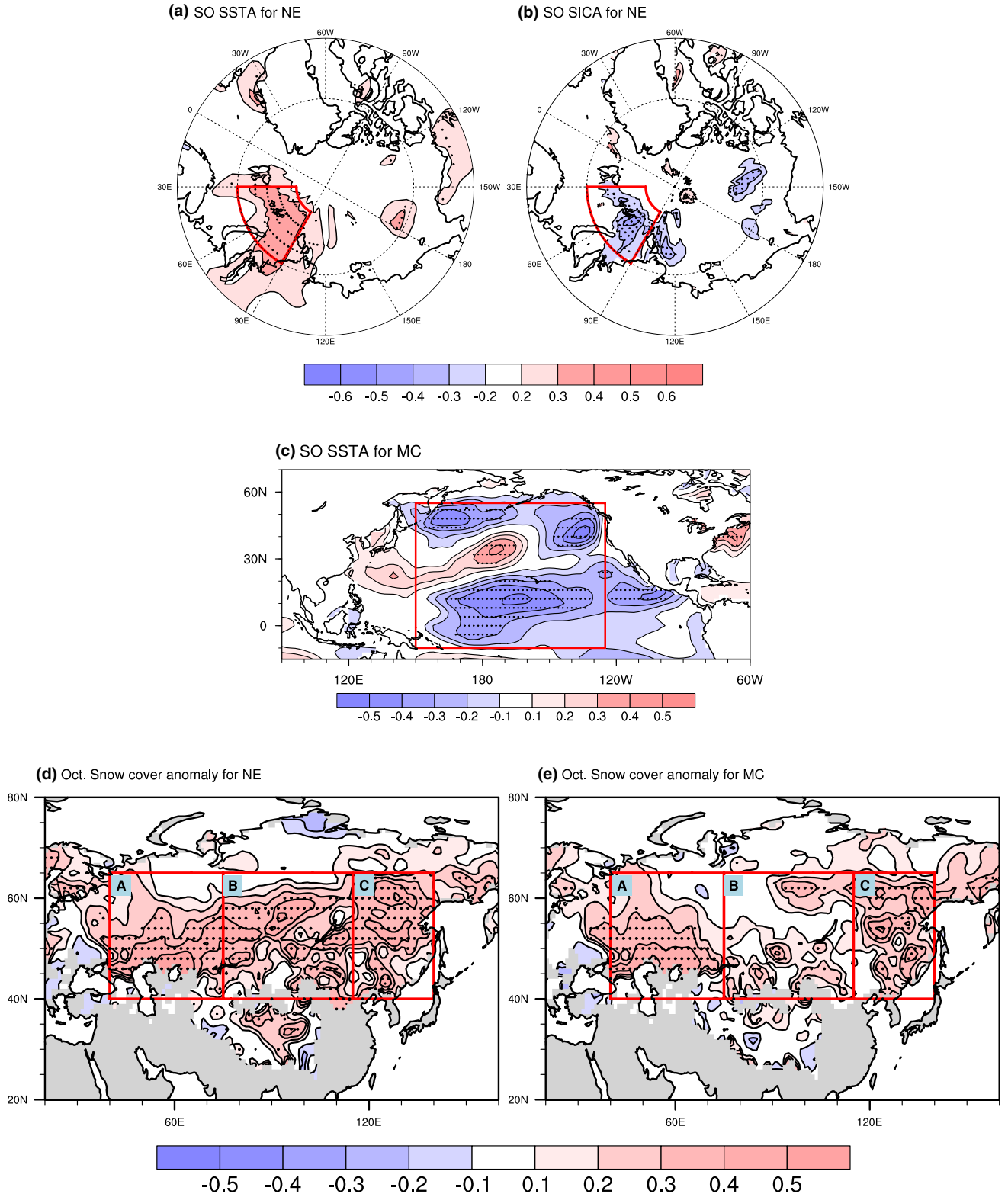

and November, possibly because of the large variability of snow cover extent in this area in October (figure not shown), and this conclusion is consistent with Jhun and Lee (2004).

In summary, we have identified two precursors (i.e., ARCT-NE and SNOW-NE) for NECD-NE, and two precursors (i.e., SNOW-MC and TNPSST-MC) for NECD-MC, respectively. The mutual correlation coefficients between

◂**Fig. 6** Fall precursory anomalies associated with the winter NECD over MC and NE. **a** Correlation maps of NECD-NE and SO (September–October) mean SST over ocean and T2m over land, **b** same as **a**, but for SO mean sea ice concentration. **c** Correlation maps between NECD-MC and SO mean SST. **d** Correlation maps of Snow cover extension in October over land and the NECD-NE, **e** same as **d**, but for the NECD-MC. *Black dots* represent the regions with correlation significant at the 95% confidence level. The *boxes* in **a** and **b** outline the regions where ARCT-NE are defined (Table 2). The *rectangular box* in **c** outline the region where the TNPSST-MC predictor is defined (Table 2). The *three rectangular boxes* marked as *A, B, C* in **d** and **e** outline the three corresponding key regions discussed in the text, and region $A+B+C$ in **d** and region $A+C$ in **e** denote regions where the SNOW-NE and SNOW-MC predictors defined, respectively (Table 2)

the two predictors for the NECD-NE are statistically insignificant (Table 3a). The two predictors TNPSST-MC and SNOW-MC are well correlated to the NECD-MC with correlation coefficients at 0.62 and 0.65, respectively.

5.2 Discussion of physical linkages between the predictors and NECDs

5.2.1 Autumn Eurasian snow cover and winter NECD in northeast and main China

Previous studies have shown the snow cover anomalies over Eurasia could influence winter circulation (Watanabe and Nitta 1998; Jhun and Lee 2004; Cohen and Fletcher 2007), but the key regions for precursory snow cover anomalies were not clearly identified. We have identified three sub-regions in Eurasia where snow cover anomalies in October are found to relate to the variation of the NECD-NE and NECD-MC, namely, snow cover region A, B, and C (Fig. 6d, e). The difference between SNOW-NE and SNOW-MC lies in the region B (Fig. 6d, e). Therefore, we further examine the potentially different influences of the snow cover over three sub-regions, A, B, and C (Fig. 6d) on winter circulations by computing partial regression coefficients. The partial regression coefficients are derived from multiple linear regression analysis with regard to the snow cover over regions A, B, C.

Figure 7a shows that an excessive snow cover in region A is related to the high anomaly over Ural mountain and enhanced Aleutian Low during winter. Similarly, an increased snow cover in C is related to the anomalous Ural High and the East Asian Trough (Fig. 7c). Meanwhile, the Mongolian-Siberian High at SLP intensifies and the ECDs increase in both the NE and MC regions (Fig. 7a, c). Thus, the snow cover extent in region A and C are selected as common precursors for both NECD-NE and NECD-MC.

Figure 7b shows that an increased snow cover extent in region B leads to a very different 500 hPa height anomalies during the winter, which is zonal symmetric and manifests anomalous polar high and the mid-high latitude low (a negative phase of AO). In fact, the October snow cover in B is most closely related with the winter AO with a correlation coefficient reaching −0.64. The negative AO phase and the northwestward shift of Aleutian Low lead the cold air into the high latitude area of Eurasian continent (Fig. 7b). Meanwhile, other studies also suggest that the October Eurasian snow cover extent modulates the January AO through a dynamical process that includes anomalous vertical propagation of Rossby wave activity (Gong et al. 2003; Cohen and Fletcher 2007; Cohen et al. 2012). Therefore, the snow cover extent in B is selected as a predictor for the NECD-NE prediction instead of for the NECD-MC.

5.2.2 Autumn tropical-North Pacific SST anomalies and NECD in main China

Apart from snow cover predictor, the NECD-MC is largely signified by the preceding autumn tropical-North Pacific SST precursor (Fig. 6c). With a set of paired coupled model experiments [(+) SST minus (−) SST], in which the anomalous SST field illustrated in Fig. 8a are nudged in September and October, we show, in Fig. 8b, the wintertime circulation anomalies associated with the tropical-North Pacific SST precursor. The autumn cooling phase TNPSST-MC precursor (Fig. 8a) signifies the Central Pacific La Niña (CP La Niña) in the ensuing winter (Fig. 8b). Correspondingly, a pair of cyclonic anomaly is clearly seen over the subtropical western Pacific and northern Indian Ocean, exerting northeasterlies over the southeastern and southern Asia, hence results in a cold winter and increased ECDs over the southern part of main China. It is also notable that there is an anomalous high over mid-high latitude region of the central Eurasian continent, and the northeasterlies on its southern flank can reinforce the cold air advection to northwest China that favors more ECDs there.

5.2.3 Autumn Arctic SST anomalies and NECD in northeast China

The mechanism of how autumn Arctic SST may influence the winter temperature over temperate East Asia (TEA) has been discussed by Luo and Wang (2016). Due to the large ocean heat capacity, the Eurasian Arctic warming in September and October can persist into the ensuing winter (Fig. 9a). The Arctic warming in winter induces high anomaly over the Ural Mountain and deepens the East Asian trough in the mid-troposphere, thus strengthening the Mongolia-Siberian High in the surface (Fig. 9a, b), favoring the cold air outbreak intrusion into primarily the northeast China. The numerical experiment made by Kug et al. (2015) has shown that the Eurasian Arctic warming in winter may induce an anticyclonic anomaly extending

Table 2 Definition of each predictor for the leading regional NECD mode

Mode	Predictor name	Meaning	Definition regions
NECD-NE	SNOW-NE	Oct. Snow cover anomalies	Snow cover (40°N–65°N, 40°E–140°E)
	ARCT-NE	SO Arctic SST anomalies	SST (75°N–85°N, 30°E–90°E)
NECD-MC	SNOW-MC	Oct. Snow cover anomalies	Snow cover (40°N–65°N, 115°E–140°E) and (40°N–65°N, 40°E–75°E)
	TNPSST-MC	SO tropical-North Pacific SST anomalies	SST (10°S–50°N, 150°E–130°W)

Table 3 The correlation coefficients between predictand, (a) NECD-NE, (b) NECD-MC, and the corresponding two predictors as well as between the two predictors during 1973–2013

(a)	SNOW-NE	ARCT-NE
NECD-NE	**0.70**	**0.49**
SNOW-NE		0.14
ARCT-NE		
(b)	SNOW-MC	TNPSST-MC
NECD-MC	**0.62**	**0.65**
SNOW-MC		**0.41**
TNPSST-MC		

The bold numbers denote statistically significant at the 99% confidence level

from the polar region to the Ural Mountain. Consequently, Rossby wave energy propagation induces downstream low pressure anomalies that deepen and westward shift the East Asian trough at 500 hPa, and this favors cold air intrusion into the lower latitude (Fig. 9a, b), which leads to extreme cold condition over the northern Asia including the Northeast China.

The linkage between the autumn Arctic sea ice concentration and the winter mean temperature was noticed by a number of previous studies (Wu et al. 1999; Inoue et al. 2012; Chen et al. 2014a, b). Wu et al. (1999) argue that heavy sea ice in the Kara Sea and the Barents Sea can excite the 500 hPa EU teleconnection pattern thus modulating the EAWM. Inoue et al. (2012) proposed that sea ice concentration in Barents Sea can affect the atmospheric baroclinicity, thus changes the frequency of the eastward propagating cyclonic systems, leading to a SLP anomaly over the Siberian coast and affecting the EAWM.

6 A Physical-empirical model for the prediction of NECDs in China

In this section, we use multi-regression to establish PEM for the simulation and the prediction of NECD and for the estimation of the associated predictability. The predictors used are the same as discussed in the previous section.

The simulation equations derived from the period of 1973–2013 are

$$\text{NECD-NE} = 3.67 \times \text{SNOW-NE} + 2.16 \times \text{ARCT-NE},$$

$$\text{NECD-MC} = 2.08 \times \text{SNOW-MC} + 2.37 \times \text{TNPSST-MC}$$

Since all predictands and predictors are normalized, the magnitude of the coefficients associated with each predictor indicate relative contributions of the corresponding predictor to the predicted NECD. As for the NE region, the snow cover extension anomaly plays a considerable larger role in predicting the NECD-NE. For the MC region, the snow cover anomaly and the Pacific SST anomaly have comparable contribution.

To evaluate the prediction skill, a 41-year cross-validated retrospective forecast is performed. The prediction models were derived by using a suite of training 38-year data (leaving 3 years data out around each target prediction year), and then apply the derived model to forecast the middle year of the three withheld years. The cross-validated correlation skills for the entire period (41 years) are 0.78 for the NECD-NE (Fig. 10a) and 0.73 for the NECD-MC (Fig. 10b).

In addition to the temporal correlation coefficient (TCC), we calculate Mean Square Skill Score (MSSS) (Murphy 1988): MSSS = 1 − MSE/MSEc, where $MSE = \frac{1}{n}\sum_{i=1}^{n}(f_i - x_i)^2$ is the mean square error (MSE) of the forecasts by the PEM, and $MSE_c = \frac{1}{n}\sum_{i=1}^{n}(x_i - \bar{x})^2$ is the MSE of the climatological forecast. The x and f denote time series of observations and forecasts, respectively. Positive (negative) skill indicates that the model's forecast is better (worse) than the climatological "forecast". The MSSS skills for seasonal forecast of the NECD-NE and NECD-MC reach 0.59 and 0.54, indicating the predictions based on the PEMs have much higher skills than the climatological forecasts (MSSS skill is zero).

The NECD forecast can be further made for each station. Two methods can be used for this downscaling prediction. In the first method, we use two forecasted indices, the NECD-NE and NECD-MC, to predict the NECD at each station. The forecast TCC skills over most stations are generally over 0.6, except for the northwest China (Fig. 11a). The MSSS skill reaches 0.4 in the middle and northeast China, but is lower for the northwest China (Fig. 11b). In the second method, we

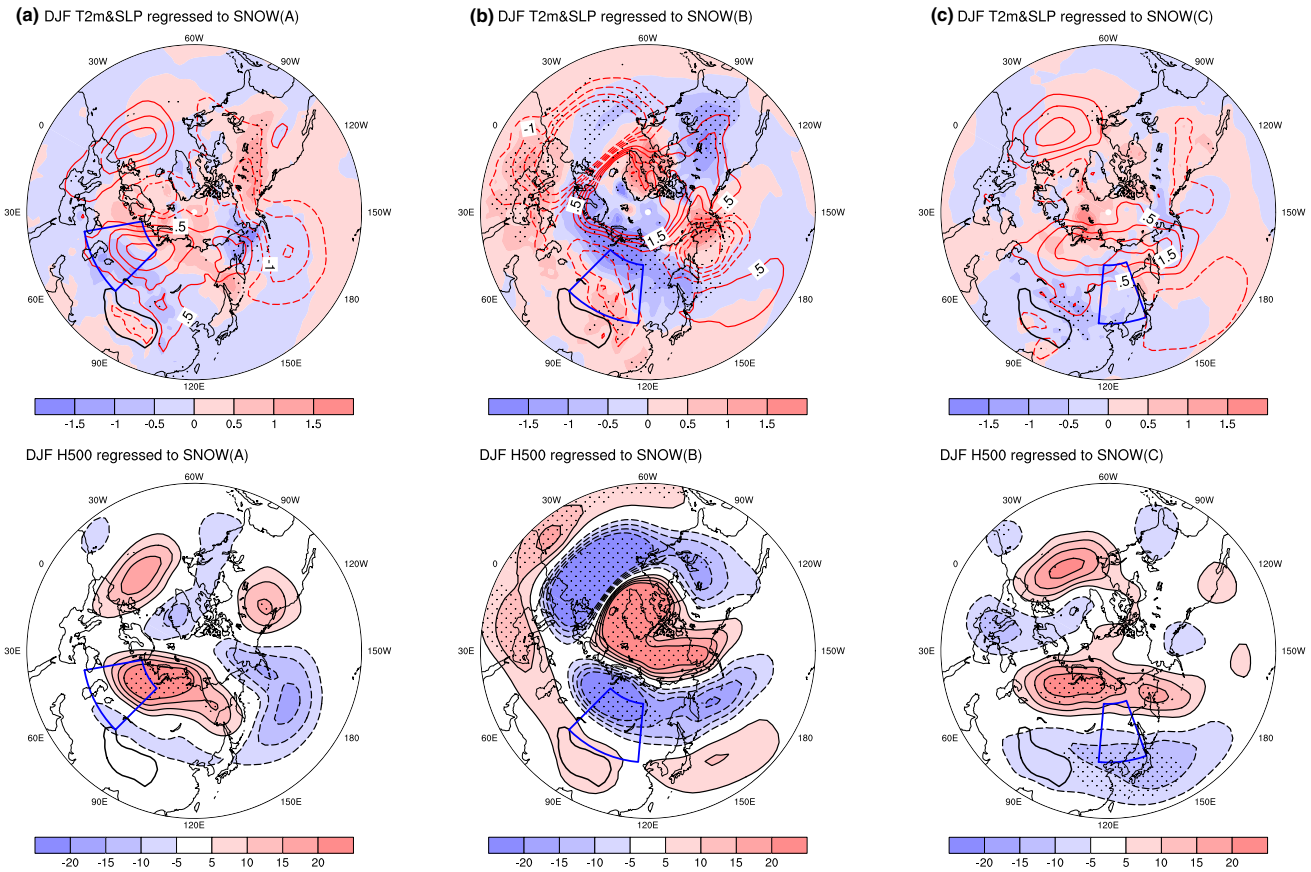

Fig. 7 The DJF anomaly fields associated with the October snow cover extension anomaly over the key region *A, B* and *C*, respectively. **a** Partial regressed T2m (*shaded*; °C), SLP (*contours*; hPa) (*upper panel*) and 500 hPa height anomalies (*lower panel*) with reference to the snow cover over the key region *A*. **b, c** The same as in **a** except for the snow cover over the key region *B*, and *C*, respectively. In the *upper panels*, the contour interval is 0.5 hPa; positive (negative) contours are *solid* (*dashed*); the zero contour is not shown. The *dots* denote regions where T2m and H500 anomalies are statistically significant at 95% confidence level. The *blue boxes* in **a–c** outline the regions of the snow cover *A, B*, and *C*, respectively

use the four predictors (Table 2) directly to derive prediction equations for each station. The forecast TCC (MSSS) skill are higher than those in the first method, reaching around 0.7 (0.5), respectively for stations over the NE and Main China.

The above PEM prediction provides an estimate of the practical predictability. The TCC skills of 0.78 for the NECD-NE and 0.73 for NECD-MC suggest about 60% (55%) of the total variance of the NECD in NE (MC) may be potentially predictable and the frequency of the extremely cold events during winter in the large domain of China is to a large extent predictable before the season begins.

7 Concluding remarks

7.1 Conclusions

We have shown that the five ENSEMBLE models' Multi-model ensemble prediction only yields a moderate, averaged temporal correlation coefficient skill of 0.23 over China during 1960–2005 (Fig. 1). For this reason, in the present study we used Physics-based empirical models (PEMs) to explore the sources and limits of the seasonal predictability and prediction method for the total number of winter extremely cold days (NECD).

To simplify the prediction problem and better detect the sources of predictability, we used a combined cluster and Rotated EOF analysis approach (Figs. 2, 3) to categorize 503 Chinese station's NECD into three quasi-homogeneous sub-regions, i.e., Northeast China (NE), Main China (MC), and Tibetan Plateau. Two regional mean NECD indices are defined for the NE and MC regions as our target predictands, the NECD-NE and NECD-MC, for the 41-year period from 1973 to 2013 (Fig. 4).

Both the NECD-NE and NECD-MC reflect Eurasian continental-scale surface air temperature anomalies (Fig. 5a), which correspond, respectively, to the Northern and Southern mode of East Asian winter monsoon

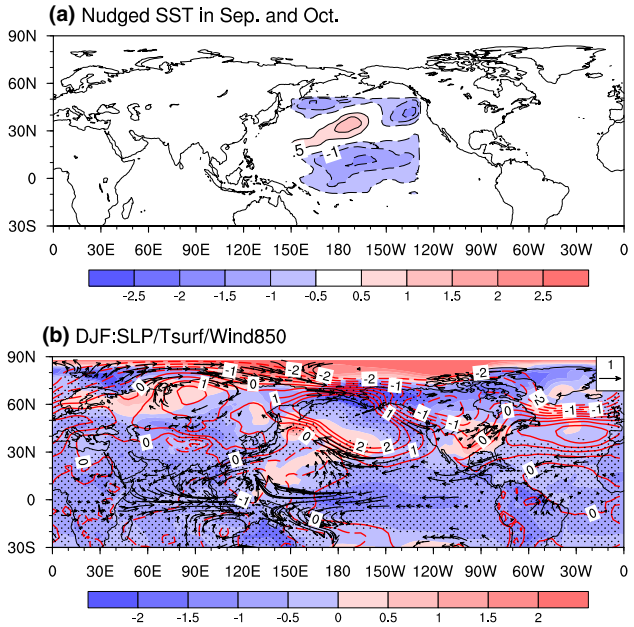

Fig. 8 Model simulated DJF anomaly fields associated with the predictor TNPSST-MC. **a** The TNPSST-MC related nudged SST field in September and October for (+) SST experiment (*shaded*; °C). **b** Differences in the ensemble mean DJF surface temperature (*shaded*; °C), surface wind (*vectors*; m s^{-1}) and SLP anomalies (*contours*; hPa) between (+) SST experiment and (−) SST experiment. The contour interval is 0.5 hPa; positive (negative) contours are *solid* (*dashed*) and zero contour is omitted. *Dots* in **b** indicate region with of SST anomalies significant at 99% confidence level. *Vectors* in **b** are shown only when values for zonal or meridional wind anomalies are significant at 90% confidence level

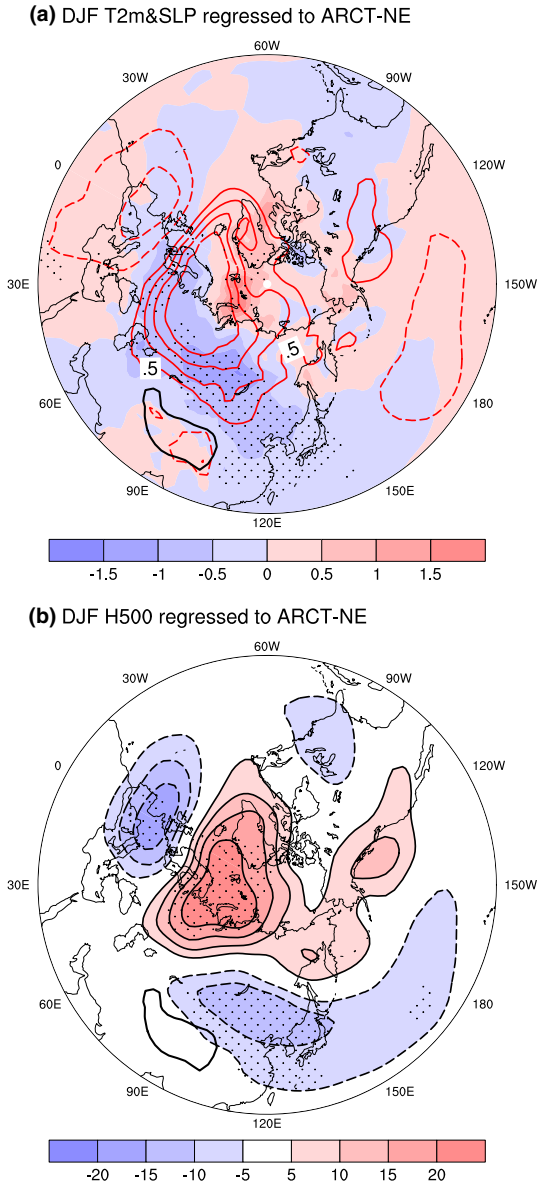

Fig. 9 Winter circulation anomalies associated with the autumn ARCT-NE predictor. **a** The regressed winter SLP (*contours*; hPa) and T2m (*shaded*; °C) anomalies with reference to autumn ARCT-NE predictor. The contour interval is 0.5 hPa and positive (negative) contours are *solid* (*dashed*) *lines*. The zero contour is not shown. **b** Same as **a**, but for the 500 hPa height anomalies (*shaded*; gpm). *Dots* in **a** and **b** indicate regressed anomalies of T2m and 500 hPa geopotential height significant at 95% confidence level, respectively

identified by Wang et al. (2010). When the NE has more ECDs, the winter circulation anomalies are characterized by an Arctic High and a zonal symmetric low pressure that are closely related to a negative phase of AO. On the other hand, for an extremely cold winter in the MC, the SLP anomalies feature a "Northern High and Southern Low" pattern over Eurasia (Fig. 5e). The common characteristics are the anomalous high over Ural Mountain and deepened EA Trough, but the corresponding anomaly locations are different.

The predictability of the NECD-NE and NECD-MC originates from the lower boundary forcing, i.e., SST and snow cover anomalies, in the previous autumn (Fig. 12). However, they have different SST and snow cover predictors. The October snow cover anomaly over Eurasian continent is the predictor for the NECD-MC, while that over the Mongolian and Siberian region (region B on Fig. 6c) is the precursor for the NECD-NE. The NECD-NE has an autumn SST predictor in the western Eurasian Arctic Ocean, which can persist into winter and induce pressure anomalies over the Ural mountain and downstream East Asia (Fig. 9). On the other hand, The NECD-MC has an autumn SST predictor in the tropical and North Pacific, which presages the development of the winter equatorial central Pacific SST anomalies that further impact winter circulations over Eurasia. Numerical experiments indicate that the northwestern Pacific anomalous cyclone and mid-high latitude Eurasia anomalous anticyclone are the key systems that bridge the precursor and more NECDs over the Main China through facilitating cold air advection into the northwest and central-southern China (Fig. 8).

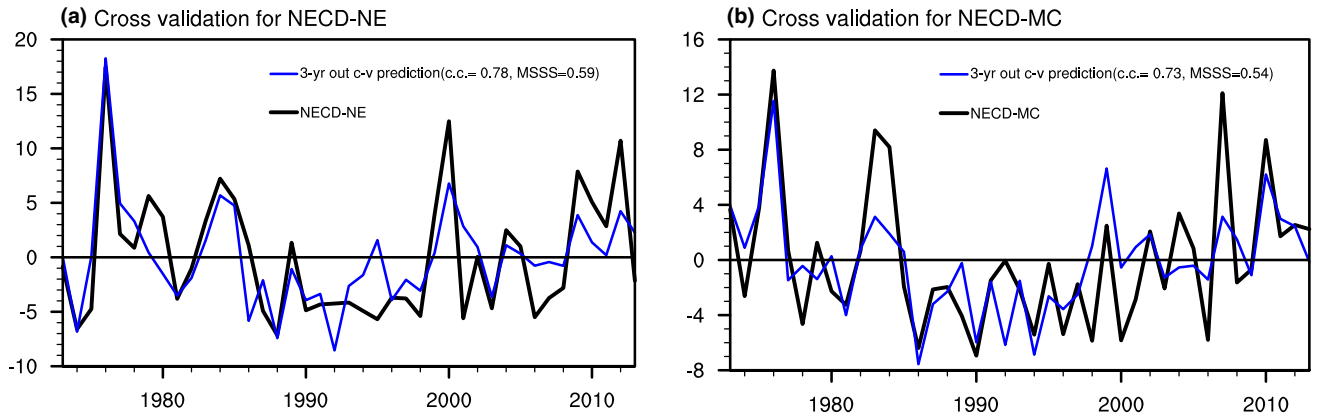

Fig. 10 Hindcast skills of the physical-empirical model (PEM) predictions. **a** The time series of observed NECD-NE (*black line*) and the predicted NECD-NE (*blue line*) with cross-validation method obtained by taking 3-year out at each prediction year. The prediction is made at the end of October (1-month lead prediction). **b** Same as **a**, but for the NECD-MC. The cross-validated prediction TCC (MSSS) skills for the NECD-NE and NECD-MC are 0.78 (0.59) and 0.73 (0.54), respectively

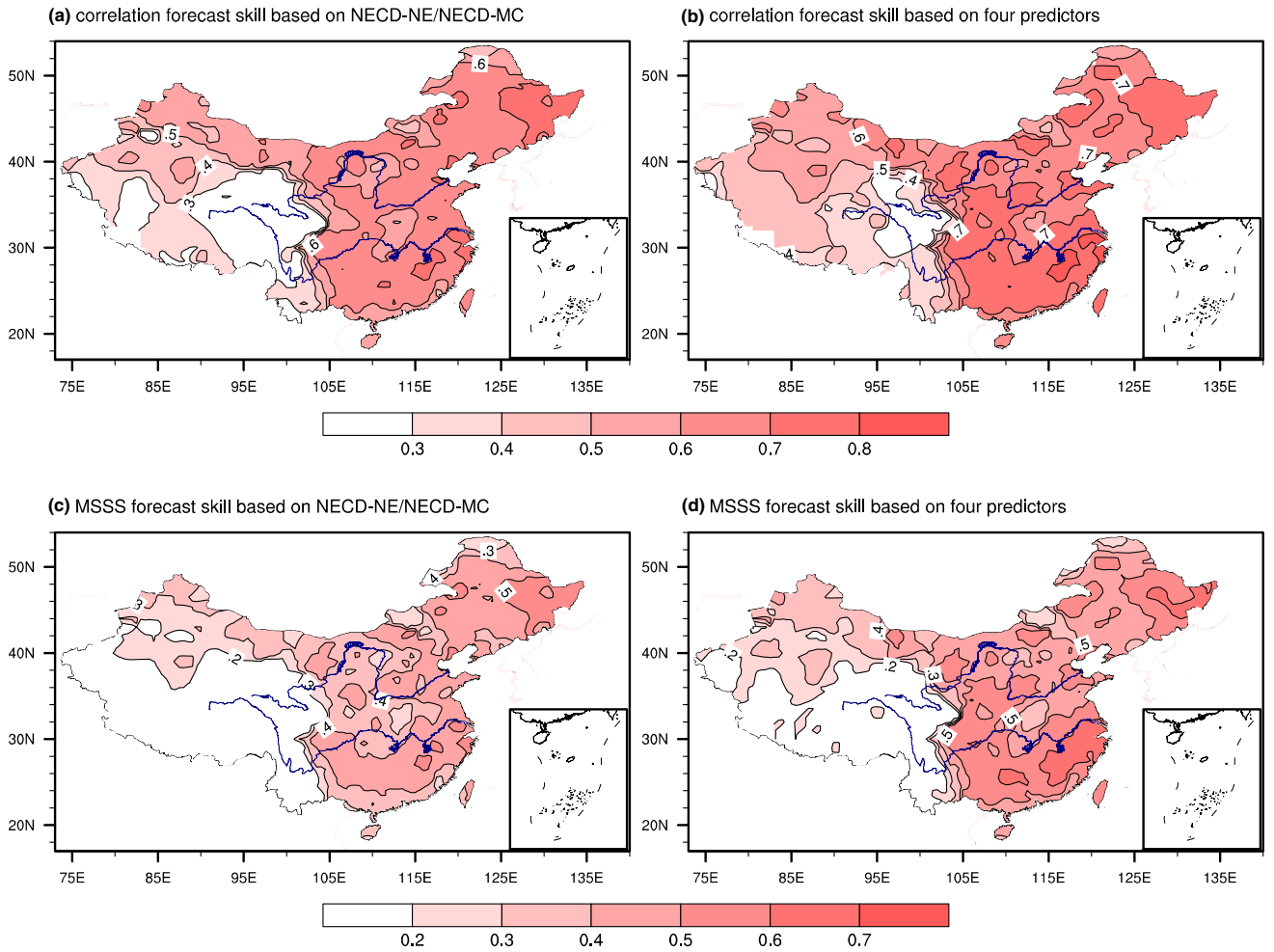

Fig. 11 Forecast skills for the winter NECD over China during 1973–2013 measured by the correlation coefficient (**a, b**) and MSSS (**c, d**). **a** Map of correlation coefficients between the observed and predicted winter ECDs at each station derived from the prediction equations based on multiple regression using the PEMs-predicted NECD-NE and NECD-MC indices. **b** Same as **a**, but the predicted NECD at each station is derived from prediction equations based on multiple regression using the four predictors in Table 2. **c** Same as **a**, except for MSSS. **d** Same as **b**, except for MSSS

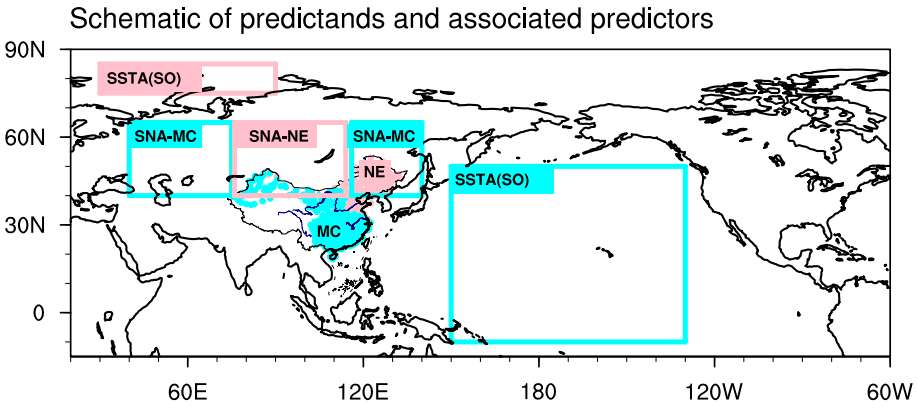

Fig. 12 Locations of the Northeast China (NE) and Main China (MC) and their associated NECD predictability source regions. *Red* and *blue dots* in China regime denote the stations in the NE and MC, respectively. *Red rectangular boxes* outline precursors for the NECD over NE and are marked as SSTA(SO) over Arctic Ocean and SNA-NE over Eurasian continent. *Blue rectangular boxes* outline precursors for the NECD over MC and are denoted as SSTA(SO) over the tropical-North Pacific Ocean and SNA-MC over the Eurasian continent

The PEMs' hindcast results suggest that about 60% (55%) of the total variance of winter NECD over Northeast China (Main China) may be predictable 1 month in advance (Fig. 10). The four predictors that are identified for the NE and MC regional indices can be used to make downscale predictions for each station. The cross-validated temporal correlation skills reach 0.70 and MSSS of 0.5 at most stations within the Main and NE China (Fig. 11).

7.2 Discussion

Use of cluster analysis to identify the regions of coherent variations of climate anomalies is shown to facilitate understanding the sources of climate predictability, identifying large scale predictors, and downscaling prediction of local anomalies.

The reason we used detrended data is that some predictors have significant trends, especially the Eurasian Arctic Ocean SST. Because these large trends are largely related to external forcing such as anthropogenic warming, for the purpose of prediction of the interannual and decadal variation, we removed the trends from these predictors. To be consistent, in the present study we also removed the linear trends from the predictands, although these trends are not significant at the 90% confidence level.

To apply the PEM to real prediction, we first calculate the four detrended and normalized autumn predictors for the NCED in the target winter using the method described in Sect. 5.1, and then put them in the established prediction equations of PEM to get the predicted detrended NECD. The second step is to calculate the trend component of the target winter NCED based on the linear trend of NECD prior to the target winter. Finally, the sum of the detrended NECD from PEM prediction and the trend component of NCED is the predicted NECD for the target year.

It is of interest to notice the differences in NECDs between the NE region in the present study and the temperate East Asia (TEA) region studied by Luo and Wang (2016). Geographically, the NE region is embedded within the TEA region (30°–50°N, 110°–140°E), but the TEA covers a much larger domain, including Korea, western Japan, the marginal seas of the western North Pacific (WNP), and part of Main China region. As a result, the physical predictors signifying NECD at the TEA region also differ from those in the NE region. For instance, the developing El Niño/La Niña is a predictor for the TEA because it includes a region of WNP, but it is not a predictor for the NE region. On the other hand, because the NE is located in the northwest part of the TEA, the Asian snow cover becomes an important predictor.

One may wonder whether the winter mean temperature is more predictable than the total number of winter extremely cold days, the NECD. We found that the winter mean temperature and NECD are highly correlated with correlation coefficients of −0.88 and −0.85 for the NE and Main China, respectively. This confirms the results of Luo and Wang (2016). They have also demonstrated that in the core region of EAWM, (a) the NECD and winter mean temperature have the same sources of predictability, and (b) predictions of the winter mean temperature and NECD using the same predictors yield comparable skills. Thus, the physical basis for the prediction of NECD is essentially the same as that for the prediction of the seasonal mean temperature.

The cross-validated retrospective forecasts suggest the NE region, even though located at higher latitude, has

higher predictability in terms of NECD than the Main China region. This is consistent with the ENSEMBLE dynamical models' result, which suggests that some robust factors are in action. This is probably because the frequency of the extremely cold events in the Northeast China are more tightly linked to negative phase of wintertime AO, for which the western Eurasian Arctic warming and enhanced snow cover over Mongolia and western Siberia in autumn are more robust precursors.

The high NECD-MC is found to be related to the preceding cooling phase of horseshore like SST anomaly pattern in the tropical and North Pacific, which signifies a winter central Pacific cooling. Even though the mechanism associated with the northwestern Pacific anomalous cyclone has been fairly well understood (Wang et al. 2000), the physical linkage between the winter anomalous anticyclone over Eurasian and the tropical and North Pacific SST anomalies in the preceding fall remains elusive.

Although the snow cover anomalies in the region A (C) in Fig. 6d, e include some different significant grid points, we find that the variations of areal averaged snow cover extension anomalies in the region A(C) are consistent, with a correlation coefficient of 0.97 (0.98). The snow cover anomaly in region B (i.e., Mongolian and southern Siberian region: 40°N–65°N, 75°E–110°E) in October is found to be uniquely related to winter AO. This specific location of snow cover anomaly differs from the previous results that focused on a vast region over the Eurasian continent (Watanabe and Nitta 1998; Cohen and Fletcher 2007). This discrepancy suggests that the seasonal predictability of the AO is worthy of further investigation. Further analysis shows the correlation between the snow cover anomaly in region A and NECD over China has dropped significantly since 1980s. This unstable relationship indicates that the snow cover A could be left out for the NECD forecast practice in the recent decades.

The spatial patterns of forecast skill show lower predictability of the NECD over the northwest China. This could be due to the fewer stations over the northwest China comparing with densely populated stations over other parts of Main China, which could result in a biased weighting of the NECD-MC index toward the central and southern China.

Acknowledgements This work has been supported by the National Natural Science Foundation of China (Grant Nos. 41420104002 and 41371209), the Global Research Laboratory (GRL) Program of the National Research Foundation of Korea Grant No. 2011–0021927, and Atmosphere–Ocean Research Center sponsored by the Nanjing University of Information Science and Technology and University of Hawaii. This is the SOEST publication 10011, IPRC publication 1253 and NUIST/ESMC publication 161.

References

Cao J et al (2015) Major modes of short-term climate variability in the newly developed NUIST Earth System Model (NESM). Adv Atmos Sci 32:585–600

Chen Z, Wu R, Chen W (2014a) Distinguishing interannual variations of the northern and southern modes of the East Asian winter monsoon. J Clim 27:835–851

Chen Z et al (2014b) Impacts of autumn Arctic sea ice concentration changes on the East Asian winter monsoon variability. J Clim 27:5433–5450

Cohen J, Fletcher C (2007) Improved skill of northern hemisphere winter surface temperature predictions based on land–atmosphere fall anomalies. J Clim 20:4118–4132

Cohen JL, Furtado JC, Barlow MA, Alexeev VA, Cherry JE (2012) Arctic warming, increasing snow cover and widespread boreal winter cooling. Environ Res Lett 7:014007

Collins D, Della-Marta P, Plummer N, Trewin B (2000) Trends in annual frequencies of extreme temperature events in Australia. Aust Meteorol Mag 49:277–292

Gong G, Entekhabi D, Cohen J (2003) Modeled northern hemisphere winter climate response to realistic Siberian snow anomalies. J Clim 16:3917–3931

Grunseich G, Wang B (2016) Predictability of Arctic annual minimum sea ice patterns. J Clim 29:7065–7088

Huffman GJ, Bolvin DT (2013) GPCP version 2.2 SG combined precipitation data set documentation. NASA, p 46. ftp://precip.gsfc.nasa.gov/pub/gpcp-v2.2/doc/V2.2_doc.pdf

Inoue J, Hori ME, Takaya K (2012) The role of Barents sea ice in the wintertime cyclone track and emergence of a warm-Arctic Cold-Siberian anomaly. J Clim 25:2561–2568

Jhun J-G, Lee E-J (2004) A new East Asian winter monsoon index and associated characteristics of the winter monsoon. J Clim 17:711–726

Kalnay E et al (1996) The NCEP/NCAR 40-year reanalysis project. Bull Am Meteorol Soc 77:437–471

Kug J-S, Jeong J-H, Jang Y-S, Kim B-M, Folland CK, Min S-K, Son S-W (2015) Two distinct influences of Arctic warming on cold winters over North America and East Asia. Nature Geosci 8:759–762

Lee J-Y, Lee S-S, Wang B, Ha K-J, Jhun J-G (2013) Seasonal prediction and predictability of the Asian winter temperature variability. Clim Dyn 41:573–587

Li J, Wang B (2015) How predictable is the anomaly pattern of the Indian summer rainfall? Clim Dyn 46:2847–2861

Li J, Wang B, Yang Y-M (2016) Retrospective seasonal prediction of summer monsoon rainfall over West Central and Peninsular India in the past 142 years. Clim Dyn 48:2581–2596

Liu K, Song W, Zhu Y (2012) A statistical prediction method for an East Asian winter monsoon index reflecting winter temperature changes over the Chinese mainland. Acta Meteorol Sin (in Chinese) 71:275–285

Luo X, Wang B (2016) How predictable is the winter extremely cold days over temperate East Asia? Clim Dyn 48:2557–2568

Luo X, Zhang Y (2015) The linkage between upper-level jet streams over East Asia and East Asian winter monsoon variability. J Clim 28:9013–9028

Murphy AH (1988) Skill scores based on the mean square error and their relationships to the correlation coefficient. Mon Weather Rev 116:2417–2424

Pepler AS, Díaz LB, Prodhomme C, Doblas-Reyes FJ, Kumar A (2015) The ability of a multi-model seasonal forecasting ensemble to forecast the frequency of warm, cold and wet extremes. Weather Clim Extremes 9:68–77

Philipp A, Della-Marta PM, Jacobeit J, Fereday DR, Jones PD, Moberg A, Wanner H (2007) Long-term variability of daily North Atlantic–European pressure patterns since 1850 classified by simulated annealing clustering. J Clim 20:4065–4095

Richman MB (1986) Rotation of principal components. J Climatol 6:293–335

Smith TM, Reynolds RW, Peterson TC, Lawrimore J (2008) Improvements to NOAA's historical merged land–ocean surface temperature analysis (1880–2006). J Clim 21:2283–2296

Storch HV, Zwiers FW (2001) Statistical analysis in climate research. Cambridge University Press, Cambridge, pp 811–812 pp

Sun S, Liu G, Song W (2014) A precursory signal for the dipole mode of winter temperature anomaly over eastern China [J]. Chin J Atmos Sci (in Chinese) 38:727–741

Thompson DWJ, Wallace JM (1998) The Arctic oscillation signature in the wintertime geopotential height and temperature fields. Geophys Res Lett 25:1297–1300

Wang L, Chen W (2010) Downward Arctic oscillation signal associated with moderate weak stratospheric polar vortex and the cold December 2009. Geophys Res Lett 37(9):L09707. doi:10.1029/2010GL042659

Wang L, Chen W (2013) The East Asian winter monsoon: re-amplification in the mid-2000s. Chin Sci Bull 59:430–436

Wang L, Chen W (2014) An intensity index for the East Asian winter monsoon. J Clim 27:2361–2374

Wang L, Lu M-M (2016) The East Asian winter monsoon. The global monsoon system: research and forecast (3rd edition), vol 5. World Scientific, Singapore

Wang B, Wu R, Fu X (2000) Pacific-East Asian teleconnection: how does ENSO affect East Asian climate? J Clim 13:1517–1536

Wang B, Wu Z, Chang C-P, Liu J, Li J, Zhou T (2010) Another look at interannual-to-interdecadal variations of the East Asian Winter Monsoon: the northern and southern temperature modes. J Clim 23:1495–1512

Wang B, Xiang B, Li J, Webster PJ, Rajeevan MN, Liu J, Ha KJ (2015) Rethinking Indian monsoon rainfall prediction in the context of recent global warming. Nat Commun 6:7154. doi:10.1038/ncomms8154

Watanabe M, Nitta T (1998) Relative impacts of snow and sea surface temperature anomalies on an extreme phase in the winter atmospheric circulation. J Clim 11:2837–2857

Weisheimer A et al (2009) ENSEMBLES: a new multi-model ensemble for seasonal-to-annual predictions—skill and progress beyond DEMETER in forecasting tropical Pacific SSTs. Geophys Res Lett 36

Wen M, Yang S, Kumar A, Zhang P (2009) An analysis of the large-scale climate anomalies associated with the snowstorms affecting China in January 2008. Mon Weather Rev 137:1111–1131

Wilks DS (2011) Statistical methods in the atmospheric sciences, vol 100. Academic, USA

Wu B, Huang R, Gao D (1999) Impact of variations of winter sea-ice extents in the Kara/Barents Seas on winter monsoon over East Asia. Acta Meteorol Sin 13:141–153

Xing W, Wang B, Yim S-Y (2014) Peak-summer East Asian rainfall predictability and prediction part I: Southeast Asia. Clim Dyn 47:1–13

Xing W, Wang B, Yim S-Y, Ha K-J (2017) Predictable patterns of the May–June rainfall anomaly over East Asia. J Geophys Res Atmos 122:2203–2217

Yang S-H, Lu R (2014) Predictability of the East Asian winter monsoon indices by the coupled models of ENSEMBLES. Adv Atmos Sci 31:1279–1292

Yim S-Y, Wang B, Xing W (2014) Prediction of early summer rainfall over South China by a physical-empirical model. Clim Dyn 43:1883–1891

Zhou W, Chan JCL, Chen W, Ling J, Pinto JG, Shao Y (2009) Synoptic-scale controls of persistent low temperature and icy weather over southern China in January 2008. Mon Weather Rev 137:3978–3991